Electron spectroscopy of dilute nitrides

2004 J. Phys.: Condens. Matter 16 S3201

(http://iopscience.iop.org/0953-8984/16/31/015)

INSTITUTE OF PHYSICS PUBLISHING JOURNAL OF PHYSICS: CONDENSED MATTER

J. Phys.: Condens. Matter **16** (2004) S3201–S3214 PII: S0953-8984(04)73706-6

Electron spectroscopy of dilute nitrides

T D Veal[1], I Mahboob[1], L F J Piper[1], T Ashley[2], M Hopkinson[3] and C F McConville[1]

[1] Department of Physics, University of Warwick, Coventry CV4 7AL, UK
[2] QinetiQ Ltd, Malvern Technology Centre, Malvern, Worcestershire WR14 3PS, UK
[3] Department of Electronic and Electrical Engineering, University of Sheffield, Mappin Street, Sheffield S1 3JD, UK

E-mail: C.F.McConville@warwick.ac.uk

Received 19 December 2003
Published 23 July 2004
Online at stacks.iop.org/JPhysCM/16/S3201
doi:10.1088/0953-8984/16/31/015

Abstract

The application of electron spectroscopies in dilute nitride semiconductor research for both chemical analysis and the determination of electronic and lattice vibrational properties is described. X-ray photoelectron spectroscopy of the nitrogen bonding configurations in dilute InN_xSb_{1-x} and InN_xAs_{1-x} alloys is presented. High resolution electron-energy-loss spectroscopy (HREELS) of the plasmon excitations in InN_xSb_{1-x} is shown to provide information on the electronic properties of the material, before and after annealing. HREELS is also used to investigate the GaN-like phonon modes in GaN_xAs_{1-x} alloys.

(Some figures in this article are in colour only in the electronic version)

1. Introduction

The substitution of nitrogen onto a few per cent of the group V lattice sites in conventional III–V semiconductors results in a large reduction in the band gap [1]. This enormous band gap bowing in 'dilute nitrides' is shown for GaNAs, InNAs and InNSb in figure 1. By contrast, the deviation from a linear variation of the band gap with composition is small in other ternary III–V alloys, also illustrated in figure 1 for GaInAs, a mixed cation alloy, and InAsSb, a mixed anion alloy. Another distinct difference between conventional III–Vs and dilute nitrides is also depicted. Normally, when a third element is added to a binary III–V to *reduce* the band gap, the lattice constant is *increased*. Conversely, the addition of nitrogen reduces the band gap while simultaneously *reducing* the lattice constant. Extensive research has recently been focused on the quaternary alloy, $Ga_{1-y}In_yN_xAs_{1-x}$, which exploits this property of dilute nitrides, allowing it to be lattice matched to GaAs with an emission wavelength in the 1.3–1.55 μm range that is important for optical communications technology [2]. Many different band gap wavelength ranges are also potentially accessible with the other less widely studied dilute nitrides.

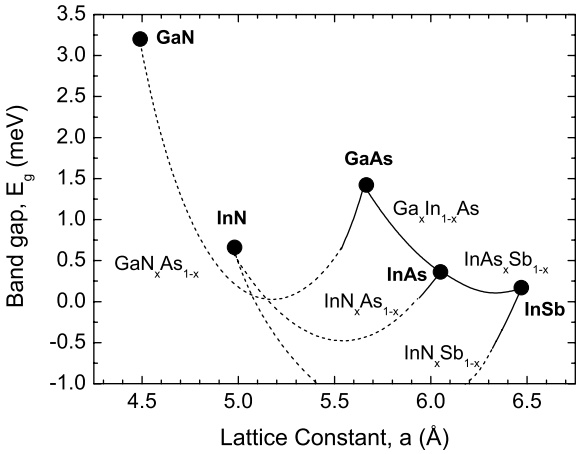

Figure 1. The band gap for several III–V semiconductors as a function of the lattice constant. A small amount of band gap bowing is exhibited by both conventional mixed cation and mixed anion III–V ternary alloys (e.g. $Ga_xIn_{1-x}As$ and $InAs_xSb_{1-x}$). By contrast, III–N_x–V_{1-x} alloys undergo enormous band gap bowing. For $0 \leqslant x \leqslant 0.1$, the dilute nitride band gaps (solid curves) are calculated using $\mathbf{k} \cdot \mathbf{p}$ theory, modified (as described in section 4) to include the effects of the localized nitrogen states. For the remaining composition range, the plotted band gap variation is merely a schematic extrapolation to illustrate the possible extent of the band gap bowing (dashed curves). Vegard's law is applied throughout to obtain the lattice constants from the compositions.

The core experimental techniques of dilute nitrides research are high resolution x-ray diffraction (HRXRD) analysis and secondary ion mass spectrometry (SIMS), to quantify the amount of nitrogen in a particular alloy, and photoluminescence, along with other optical techniques, to determine the band gap. Amongst the numerous other techniques that can be exploited to elucidate the properties of dilute nitrides are electron spectroscopies, including ultraviolet photoelectron spectroscopy (UPS), x-ray photoelectron spectroscopy (XPS) and high resolution electron-energy-loss spectroscopy (HREELS). Photoemission spectroscopies have been extensively used to probe the interface electronic properties of conventional III–V semiconductors, such as Schottky barrier heights and heterojunction band offsets [3, 4], but have yet to be widely applied to dilute nitrides [5]. We have used two of these electron spectroscopies, XPS and HREELS, to investigate the nitrogen bonding configurations and collective excitations in dilute nitrides, concentrating on the less widely studied narrow gap dilute nitrides.

In contrast to the extensive research undertaken on GaNAs and GaInNAs alloys, there have been relatively few investigations of dilute nitride alloys of the narrow gap III–Vs, which have the potential to compete with HgCdTe in far-infrared applications, such as thermal imaging and detection of environmentally important gases [6]. Alloying nitrogen with InSb can extend the cut-off wavelength from 7 μm at 300 K into the 8–12 μm atmospheric transition band where gases such as SO_2, NH_3, O_3 and CO_2 all have absorption lines [7]. Indeed, time-resolved optical measurements have been used to observe an absorption edge of 11 μm at 290 K in an alloy with a nominal composition from SIMS analysis of $InN_{0.035}Sb_{0.965}$ [8]. While only a few studies of the properties of bulk InNAs epilayers exist [9, 10], laser structures with both single and multiple InNAs/InGaAs(P)/InP quantum wells have been successfully fabricated for 2–5 μm mid-infrared applications [11, 12]. Comprehensive characterization of InNAs is also desirable as it is one of the components of GaInNAs alloys. Enhanced understanding of this technologically important quaternary alloy can be provided by investigating both GaNAs and InNAs alloys.

In this short review, we describe the application of these two electron spectroscopies to the study of dilute nitrides, using detailed examples from our own research. Section 2 contains the details of the epitaxial growth of the samples used. In section 3, two examples of XPS of nitrogen bonding configurations in InN_xSb_{1-x} and InN_xAs_{1-x} are presented. HREELS of plasmon excitations is shown, in section 4, to provide information on electronic properties of InN_xSb_{1-x} alloys. Section 5 describes a HREELS investigation of phonon excitations in GaN_xAs_{1-x} alloys. In the final section, conclusions from the preceding electron spectroscopy results are outlined.

2. InNSb, InNAs and GaNAs: epitaxial growth

The InN_xAs_{1-x} and GaN_xAs_{1-x} samples were grown by solid-source molecular beam epitaxy (MBE) at the EPSRC National Facility for III–V Technologies, using a turbo-pumped VG 80 system equipped with an Oxford Applied Research (OAR) HD25 RF plasma nitrogen source on Zn-doped p-type InAs(001) and semi-insulating GaAs(001) substrates, respectively. A regulated supply of purified nitrogen gas was provided to the RF source by means of a piezoelectric-controlled leak valve. The samples were grown with a substrate temperature of 375 °C. The nitrogen content of the InN_xAs_{1-x} sample used in the XPS study was determined by means of XRD to correspond to $x = 0.028$. The XRD of the particular GaN_xAs_{1-x} epilayer used in the HREELS work indicated a composition of $GaN_{0.104}As_{0.896}$. The layer thicknesses were 300 nm for both alloys and the layers were relaxed.

The InN_xSb_{1-x} samples were grown at QinetiQ Ltd, Malvern, UK, on an InSb buffer layer on semi-insulating GaAs(001) substrates by solid-source MBE, using a VG Semicon V80H system, equipped with an Astex AX4300 electron cyclotron resonance (ECR) plasma nitrogen source. Hydrogen was also introduced to the ECR source to enable the plasma to be sustained at low nitrogen pressures. The samples were grown with a substrate temperature of 380 °C. The total nitrogen content of the InN_xSb_{1-x} samples was determined by SIMS. Further details of the sample growth have been presented elsewhere [6]. The surfaces of the InN_xSb_{1-x}, InN_xAs_{1-x} and GaN_xAs_{1-x} epilayers were prepared *in situ* for the electron spectroscopy analysis by a two-stage atomic hydrogen cleaning (AHC) process [13]. This consisted of a 5–10 kL dose of H_2 at room temperature followed by a 5–10 kL dose at a sample temperature of 300 °C for the InN_xSb_{1-x} and InN_xAs_{1-x}, and 350 °C for the GaN_xAs_{1-x}. Each 5–10 kL dose took 20–40 min using a hydrogen gas pressure of $\sim 5 \times 10^{-6}$ mbar. The molecular hydrogen was thermally cracked to atomic hydrogen with an efficiency of ∼50%, using an OAR TC-50 thermal gas cracker.

3. Nitrogen bonding configurations in III–N–V alloys

Evidence of non-substitutional nitrogen in III–N_x–V_{1-x} alloys has been provided by comparison of data from HRXRD analysis and SIMS. While SIMS measures the total nitrogen content irrespective of the location of the nitrogen atoms, HRXRD analysis gives the change in the lattice constant caused by substitution of nitrogen on anion lattice sites. Nitrogen concentrations measured by SIMS in GaN_xAs_{1-x} have been found to exceed those determined using HRXRD by up to 30% for $x \geqslant 2.5\%$, indicating the presence of significant concentrations of non-substitutional nitrogen [14, 15]. Using XPS and ion channelling experiments, Spruytte *et al* [16] confirmed the existence of interstitial nitrogen in GaN_xAs_{1-x} grown by MBE for $x \geqslant 2.9\%$. Upon rapid thermal annealing (60 s at 760 °C), all of the nitrogen was found to be located substitutionally on anion lattice sites.

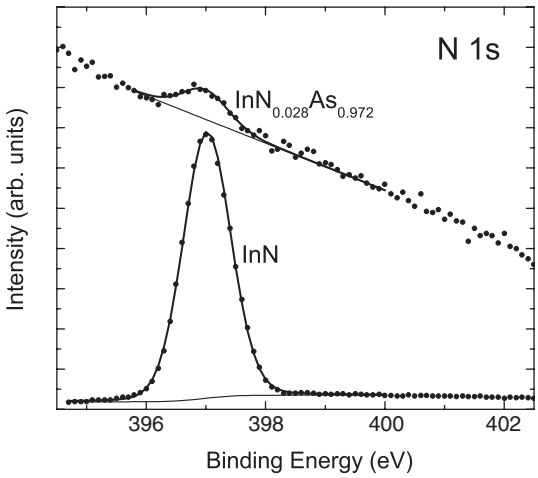

Figure 2. X-ray photoelectron spectra (dots) of the N 1s core level in $InN_{0.028}As_{0.972}$ and InN. Both N 1s spectra are fitted (solid curves) with a single component at a binding energy of 397.0 eV, indicating that all the nitrogen is bonded solely to indium.

The nitrogen content determined by SIMS was also found to exceed that indicated by XRD analysis in MBE-grown InN_xSb_{1-x} alloys [7]. Here, the results of an XPS investigation of the nitrogen bonding configurations in MBE-grown InN_xSb_{1-x} and InN_xAs_{1-x} are presented. XPS analysis of the In 3d, As 2p and 3d, Sb 3d, C 1s, O 1s and N 1s core level spectra was performed using a Scienta ESCA300 spectrometer at the National Centre for Electron Spectroscopy and Surface Analysis, Daresbury Laboratory, UK. This incorporates a rotating anode Al Kα x-ray source ($h\nu = 1486.6$ eV), x-ray monochromator and 300 mm mean radius spherical-sector electron energy analyser and parallel electron detection system. The analyser was operated with 0.8 mm slits and at pass energies of 150 eV for the InNAs and InN spectra and 500 eV for the InNSb spectra. Gaussian convolution of the analyser broadening with an effective linewidth of the 0.27 eV for the x-ray source gives effective instrument resolutions of 0.45 eV for a pass energy of 150 and 0.85 eV for a pass energy of 500 eV. Binding energies are referenced to the Fermi level of an ion bombarded silver sample which is regularly used to calibrate the spectrometer.

The N 1s XPS spectrum from an InN_xAs_{1-x} sample, with a composition determined from XRD of $InN_{0.028}As_{0.972}$, is shown in figure 2. The N 1s region recorded from an InN 'reference' sample is also shown to illustrate the binding energy of 397.0 eV of N 1s photoelectrons from nitrogen bonded to indium. The steep sloping background of the N 1s spectrum from InNAs is the high binding energy tail of the As $L_3M_{23}M_{45}$ Auger peaks at between 350 and 390 eV. The small peak at a binding energy of 397.0 eV is associated with nitrogen bonded to indium. No other chemically shifted N 1s components are present, indicating the absence of other nitrogen bonding configurations in the InNAs. The InN and InNAs spectra have been curve fitted using a Shirley background and Voigt functions each with a full width at half-maximum of 0.9 eV, consisting of 20% Lorentzian and 80% Gaussian lineshapes. Both spectra are well fitted by a single peak at 397.0 eV, confirming that the only nitrogen bonding configuration in the InNAs is N–In bonding.

The N 1s XPS spectra from an InN_xSb_{1-x} sample, with a nominal nitrogen content of 1% from SIMS analysis, are shown in figure 3. All of the spectra have again been fitted with a Shirley background and a series of Voigt functions each with a full width at half-

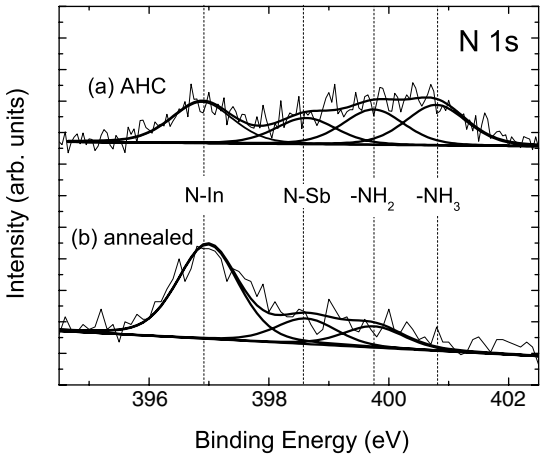

Figure 3. X-ray photoelectron spectra (thin curves) of the N 1s core level of InNSb with 1% nitrogen as determined by SIMS, recorded (a) after atomic hydrogen cleaning (AHC) and (b) after annealing at 300 °C for 8 h. The curve fitting (thick curves) of the separate chemically shifted components of the spectra is also shown.

maximum of 1.2 eV. Additionally, in the curve fitting, the position of each chemically shifted component was constrained to be at the same binding energy for all spectra recorded from several InN_xSb_{1-x} samples. After AHC, there was no observable intensity in the C 1s region, no oxide components apparent in the In 3d or Sb 3d region, and no O 1s peak was visible, indicative of complete removal of the native oxides and the hydrocarbon contamination. The N 1s region recorded after AHC is shown in figure 3. The peak at 396.9 eV is due to N–In bonding [17]; that is, N located substitutionally on group V sites, which causes the band gap reduction in dilute III–N–V materials. By analogy with the binding energies of N bonded to P in InP [17], the peak at 398.6 eV is assigned to N–Sb bonding. The peaks at 399.7 and 400.7 eV are due to $-NH_2$ and $-NH_3$ complexes, respectively [18, 19]. The area of the N–In component is approximately 30% of the total N 1s spectrum. The 'active' nitrogen content in this sample is therefore estimated, using the total nitrogen concentration from SIMS, to be 0.3%.

The N 1s spectrum recorded after annealing (8 h at 300 °C) is shown in figure 3(b). The $-NH_3$ peak is no longer present and the $-NH_2$ peak intensity has decreased. The N–Sb peak has remained unchanged, and the N–In peak has increased in intensity. These changes suggest that the annealing process has removed hydrogen from the N–H complexes and increased the degree of anion substitution. The total area of the N 1s peaks remained constant, indicating that no nitrogen was removed by annealing. The area of the N–In component is approximately 70% of the total N 1s spectrum, indicating that the 'active' nitrogen content after this annealing treatment is 0.7%. These determinations of the nitrogen content are used to interpret the HREELS data on the electronic properties of InN_xSb_{1-x} presented in section 4.

4. Plasmon excitations in III–N–V alloys

The electronic properties of dilute nitride epilayers can be investigated by using inelastic electron scattering to probe the collective excitations of the conduction band electrons [13, 20]. The energy of these plasmon excitations, ω_p, is related to the electron density and effective

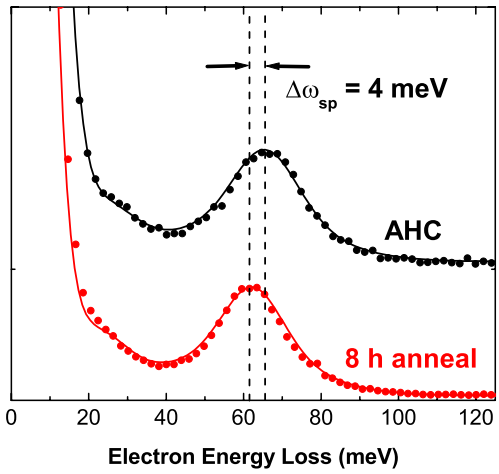

Figure 4. Experimental specular HREEL spectra (dotted curves) recorded using 30 eV electrons from InN_xSb_{1-x} grown by MBE after (a) atomic hydrogen cleaning (black, top); and (b) AHC and annealing at 300 °C for 8 h (red, bottom). Semiclassical dielectric theory simulations of the spectra are also shown (solid curves).

mass by

$$\omega_p = \left(\frac{ne^2}{\epsilon_0\epsilon(\infty)m_F^*}\right)^{1/2} \tag{1}$$

where n is the conduction electron density, e is the electronic charge, ϵ_0 is the permittivity of free space, $\epsilon(\infty)$ is the high frequency dielectric constant and m_F^* is the effective mass at the Fermi level. In HREELS, monoenergetic low energy electrons exchange energy and momentum with the long wavelength (100–1500 Å) dipole fields of the plasmon excitations. The probing electrons do not enter the sample and are specularly reflected from the sample surface into an energy analyser to produce energy-loss spectra. By varying the energy of the probing electrons, the wavevector transfer parallel to the surface is altered and the electron plasma at depths of between 100 and 1500 Å can be surveyed [21]. This allows both the surface space-charge region and the bulk of epilayers to be investigated.

In this case, HREELS has been employed to probe the electronic structure in the near-surface region of InN_xSb_{1-x} alloys as a function of annealing. The HREELS experiments were performed using a specular scattering geometry with an incident and scattered polar angle of 45°. The resolution of the HREEL spectrometer determined from the full width at half-maximum of the elastic peak was 12 meV.

Specular HREEL spectra recorded using an incident electron energy of 30 eV from InN_xSb_{1-x} are shown in figure 4 following both AHC and an 8 h anneal. The two features of these spectra are a shoulder on the elastic peak at 23 meV due to Fuchs–Kliewer surface phonon excitations (discussed in detail for GaN_xAs_{1-x} in section 5), and the peak at higher loss energy (60–70 meV) due to conduction band electron plasmon excitations. The plasmon peak position decreased from 65.5 meV for the AHC InN_xSb_{1-x} epilayer to 61.5 meV after the 8 h anneal. HREEL spectra recorded over an incident electron energy range of 7–60 eV were simulated using semiclassical dielectric theory [22]. Simulations of the spectra are required to obtain the true plasma frequency from the spectra because the observed plasmon peak position is influenced by the band bending, spatial dispersion and plasmon damping. The

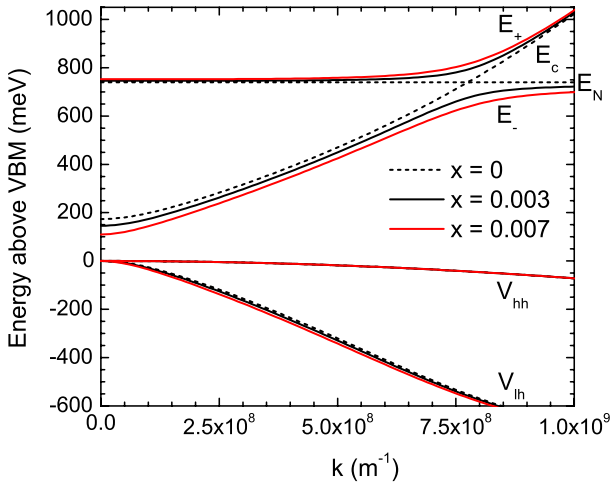

Figure 5. The dispersion of the conduction subbands (E_+ and E_-) and light and heavy hole valence bands ($V_{\rm lh}$ and $V_{\rm hh}$) calculated for InN_xSb_{1-x} with $x = 0.003$ (solid black curve, lower E_+ band and upper E_- band) and 0.007 (solid red curve, upper E_+ band and lower E_- band) from a 5×5 $\mathbf{k}\cdot\mathbf{p}$ Hamiltonian incorporating the nitrogen level. The split-off valence band is also included (but is not shown here). The conduction band profile for InSb, $E_{\rm c}$, calculated from a 4×4 $\mathbf{k}\cdot\mathbf{p}$ Hamiltonian, is plotted for comparison (dashed curve), along with the nitrogen level, $E_{\rm N}$, at 740 meV (dashed curve).

plasma frequency used in the simulations can then be used, along with calculations of the semiconductor statistics, to find the corresponding carrier concentration from equation (1). A two-layer model was used, consisting of a 70 Å thick plasma-free depletion layer and a semi-infinite bulk layer, where each layer has its own frequency- and wavevector-dependent hydrodynamic dielectric function:

$$\epsilon(\omega,q)=\epsilon(\infty)\left[1+\frac{(\epsilon(0)-\epsilon(\infty))\omega_{\rm TO}^2}{\epsilon(\infty)(\omega_{\rm TO}^2-\omega^2-{\rm i}\omega\gamma)}-\frac{\omega_{\rm p}^2}{\omega^2-\beta^2q^2+{\rm i}\omega/\tau}\right] \qquad (2)$$

where ω is the frequency, $\epsilon(0)$ and $\epsilon(\infty)$ are the static and high frequency dielectric constants, $\omega_{\rm TO}$ and γ are the transverse optical phonon frequency and phonon damping coefficient, $\omega_{\rm p}$ and τ are the plasma frequency (zero in the depletion layer) and plasmon lifetime, and β is the spatial dispersion coefficient.

The bulk plasma frequencies used in the simulation of the spectra from the InN_xSb_{1-x} epilayer recorded after AHC and an 8 h anneal were 68.5 and 65.5 meV, respectively. The observed plasmon peaks in the HREEL spectra occur at loss energies lower than the bulk plasma frequency because of the effect of the depletion layer. The plasmon lifetime used to simulate the 60 eV spectrum decreased from 0.064 ps for the AHC InN_xSb_{1-x} alloy to 0.048 ps after annealing for 8 h.

To translate the plasma frequencies extracted from the HREELS simulations of InN_xSb_{1-x} before and after annealing to carrier concentrations requires knowledge of the band structure. The introduction of nitrogen into a III–V semiconductor results in the formation of a narrow resonant nitrogen band that is situated close to the conduction band edge. The interaction of the extended Γ states of the conduction band of the host semiconductor with the localized N-induced resonant states results in the formation of two non-parabolic subbands E_- and E_+ whose dispersion is modelled using a $\mathbf{k}\cdot\mathbf{p}$ Hamiltonian [23, 24]. The E_- band has mainly

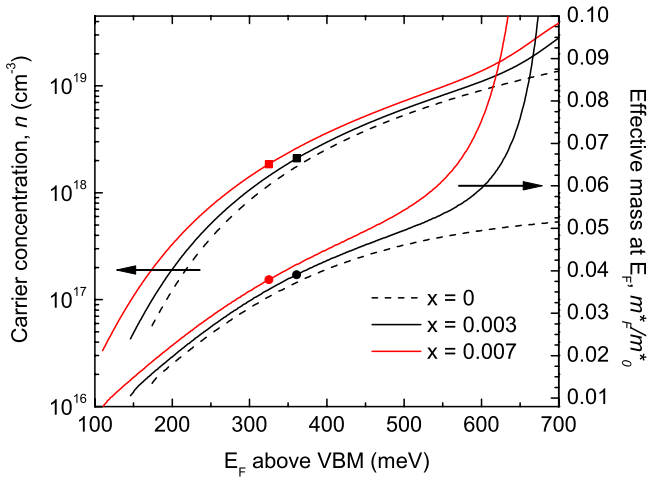

Figure 6. The effective mass at the Fermi level and the carrier concentration calculated as a function of the Fermi level for InN_xSb_{1-x} with $x = 0$ (dashed curve), 0.003 (black curves, lower solid lines) and 0.007 (red curves, upper solid lines). The black and red dots denote the particular values of the effective mass and carrier concentration before and after annealing, respectively.

conduction band-like character, whereas the E_+ subband is due to the E_N-like states. The parameters for the $\mathbf{k}\cdot\mathbf{p}$ Hamiltonian have been determined by fitting the resulting $E_\pm$ subbands to the tight binding band structure of InN_xSb_{1-x}. Details of the tight binding calculation can be found in [23] and references therein. The dispersion of the $E_\pm$ subbands can be determined by finding the eigenvalues of the 2×2 determinant

$$\begin{vmatrix} E_M - E & \beta\sqrt{x} \\ \beta\sqrt{x} & [E_N - (\alpha+\gamma)x] - E \end{vmatrix} = 0 \tag{3}$$

where $\alpha = 2.44$ eV, $\beta = 1.99$ eV, $\gamma = 2.47$ eV, $E_N = 0.74$ eV is the nitrogen level, and E_M is the host conduction band [25]. The change in the nitrogen level due to the increased concentration of N pairs with increasing x content is accounted for by γ in the above expression [24]. However, this becomes a 5×5 Hamiltonian when conventional $\mathbf{k}\cdot\mathbf{p}$ theory is included to account for the intrinsic non-parabolicity of the host InSb, due to the interaction between the valence bands and the conduction band.

The conduction band profiles for InN_xSb_{1-x} are shown in figure 5 for $x = 0$, 0.003 and 0.007 that have been calculated from the conventional and modified $\mathbf{k}\cdot\mathbf{p}$ Hamiltonians. The conduction band dispersion in InN_xSb_{1-x} is significantly different from that in InSb. The interaction of the nitrogen level with the conduction band causes the band gap to decrease as x is increased. The conduction band also undergoes a distinct flattening as it approaches the nitrogen level, resulting in enhanced effective masses at large wavevectors.

The electron dynamics (that is, the interdependence of the plasma frequency, ω_p, the carrier concentration, n, and the effective mass at the Fermi level, m_F^*) can consequently be calculated by manipulating the E_- conduction band dispersion relation calculated for InN_xSb_{1-x}. This is achieved by first numerically integrating the product of the Fermi–Dirac distribution and the density of states in the conduction band to determine the concentration of conduction electrons. Further, the effective mass can be calculated as a function of the Fermi level by exploiting its dependence on the curvature of the conduction band. Finally, the results of the first two calculations are then used to compute the plasma frequency using equation (1), where

Table 1. The composition (from SIMS and XPS) and electronic properties of the InN_xSb_{1-x} sample before and after annealing. The values correspond to the bulk plasma frequencies obtained from the simulations of the HREEL spectra. They were determined from the semiconductor statistics calculated from the $\mathbf{k} \cdot \mathbf{p}$ band structure from a 5×5 Hamiltonian.

	Unannealed	Annealed
x	0.003	0.007
E_g (meV)	146	110
λ (μm)	8.5	11.3
ω_p	68.5	65.5
n (10^{18} cm^{-3})	2.1	1.8
m_F^*	0.0391	0.0379
E_F above VBM (meV)	361	325

the mass of the free carriers forming the plasma is that at the Fermi level. The result of these calculations with $x = 0$, 0.003 and 0.007 for InN_xSb_{1-x} is shown in figure 6. The electronic properties of the InN_xSb_{1-x} sample before and after annealing are presented in table 1.

These annealing-induced changes in the electronic properties can be explained in terms of the observed changes in nitrogen bonding configurations induced by annealing (described in section 3). The changes in nitrogen bonding observed by means of XPS, which has a maximum effective probing depth of ∼60 Å, are assumed to be representative of the changes that occur over the probing depth of HREELS of 100–1000 Å. The reduction of the plasma frequency is due to a reduction of the conduction electron density. The high carrier density in the unintentionally doped samples is due to nitrogen plasma-induced damage [6], with Sb vacancies acting as donors. Annealing may result in the repair of some of these defects, lowering the donor density and the electron concentration. The reduced electron density could also be due to an increased concentration of acceptors. The reduced plasmon lifetime suggests an increase in the density of ionized impurities, enhancing the scattering rate.

The XPS results demonstrated that annealing removes hydrogen from N–H complexes, leaving more N bonded to In and increasing the x value from 0.003 to 0.007 in the alloy composition InN_xSb_{1-x}. Both experimental and theoretical studies have shown that N is an isoelectronic acceptor in GaNP, GaNAs and GaInNAs [26, 27] and that N–H complexes are electrically inactive [26, 28]. Our results suggest that H and N have the same effect in InNSb. Upon annealing, H is removed from neutral N–H complexes and diffuses out of the material. This leaves a greater concentration of N acceptors (electron traps) which results in a decreased conduction electron density and reduced plasma frequency. The additional acceptors also cause enhanced ionized impurity scattering, reducing the plasmon lifetime.

5. Phonon excitations in III–N–V alloys

In addition to providing information about the collective excitations of the conduction electrons, HREELS can also be used to probe the collective excitations of the lattice in III–V semiconductors. Specifically, in the specular reflection scattering geometry where the dipolar interaction regime dominates the inelastic electron scattering, the phonon excitations probed are long wavelength optical surface phonons that are known as Fuchs–Kliewer (FK) modes, their existence having been theoretically predicted by Fuchs and Kliewer [29]. In these long wavelength optical surface phonons, the cation and anion sublattices vibrate in opposite phase [30]. Both GaAs-like and AlAs-like FK phonon modes have previously been observed by HREELS in $Al_xGa_{1-x}As$ alloys [31, 32]. Bulk phonons, that have been extensively studied

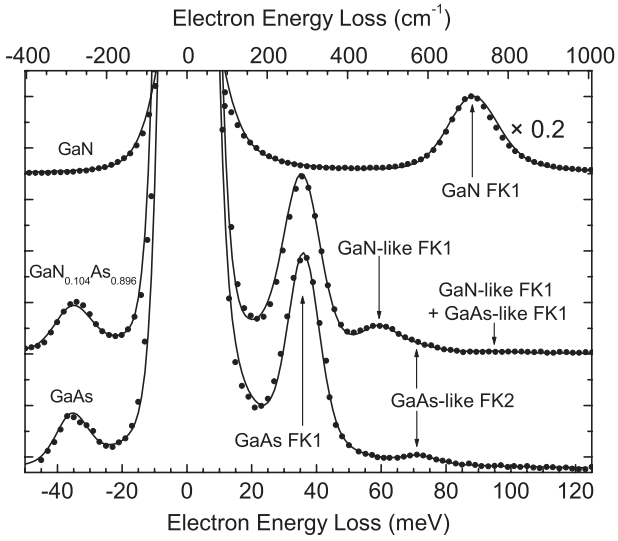

Figure 7. Specular HREEL spectra recorded with an incident electron energy of 10 eV from GaAs, $GaN_{0.104}As_{0.896}$ and GaN (points) and the corresponding dielectric theory simulations (solid curves). The intensity of the GaN spectrum is shown multiplied by 0.2 to fit in the extremely intense GaN FK phonon peak. The parameters used in the simulations of all of the spectra are given in table 2.

in III–V materials by Raman scattering, have vibrational frequencies similar to those of FK modes, but they are inaccessible to HREELS in reflection geometry. Raman scattering has also been used to investigate bulk phonon modes in dilute nitride alloys. For example, in GaN_xAs_{1-x} alloys, the Raman spectra exhibit a two-mode behaviour, where the GaAs-like longitudinal optical phonon peak red shifts as x is increased, while the GaN-like phonon mode blue shifts [33]. Here we present an HREELS study of the FK phonon spectra of $GaN_{0.104}As_{0.896}$ and compare them with spectra of the FK phonons in GaAs and GaN.

A set of HREEL spectra recorded from GaAs, $GaN_{0.104}As_{0.896}$ and GaN with an electron energy of 10 eV are compared in figure 7. The main feature in the GaAs spectrum (to the right of the elastic peak) is an intense loss peak at 35.9 meV. This peak is assigned to the GaAs Fuchs–Kliewer surface optical phonon [34]. The energy-gain peak (to the left of the elastic peak) at −35.4 meV is related to the corresponding energy-loss peak by the Boltzmann factor, $\exp(\hbar\omega/\mathrm{kT})$ [30]. Additionally, an overtone peak (FK2) can be seen at 71.8 meV, twice the loss energy of fundamental FK1 mode. The same FK phonon features appear in the GaN HREEL spectrum, but with the single-phonon loss peak at 88.0 meV. The positions of the multiple-phonon peaks for all three samples are given in table 2.

The $GaN_{0.104}As_{0.896}$ HREEL spectra exhibit both GaAs-like and GaN-like FK phonon peaks. The GaAs-like FK1 phonon peak has shifted slightly down in loss energy to 35.5 meV and is also less intense than in the pure GaAs spectrum. The GaN-like FK1 phonon peak is at a loss energy of 59.4 meV (479 cm^{-1}). This is very close to the LO_2 bulk phonon band at 58.2–58.9 meV, previously observed by Raman scattering in GaN_xAs_{1-x} for $x \leqslant 0.05$ [35]. This phonon feature in the Raman spectra is also referred to as a local vibrational mode (LVM) since it is associated with local Ga–N vibrations in what is predominantly a GaAs lattice [36]. Similarly, the GaN-like FK phonon mode frequency observed in $GaN_{0.104}As_{0.896}$ is significantly lower than the FK phonon frequency in pure GaN because it is the localized mode frequency

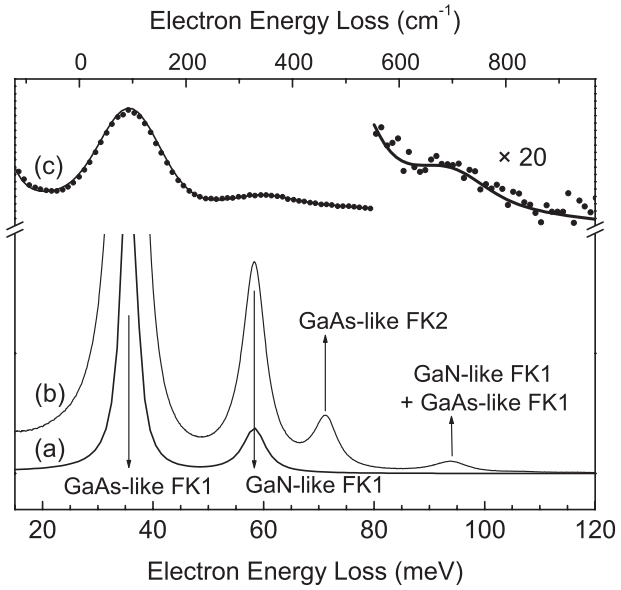

Figure 8. The stages of the semiclassical dielectric theory simulation process: (a) the single-scattering classical loss spectrum; (b) the multiple-scattering spectrum; and (c) the full 10 eV simulation (solid curve). Also shown with spectrum (c) is the 10 eV experimental data (dotted curve).

Table 2. Semiclassical dielectric theory simulation parameters and the GaAs-like and GaN-like FK phonon mode frequencies observed in the HREEL spectra from GaAs, $GaN_{0.104}As_{0.896}$ and GaN.

	GaAs	$GaN_{0.104}As_{0.896}$	GaN
GaAs FK1 (meV)	35.9	35.5	—
GaAs FK2 (meV)	71.8	71.0	—
GaN FK1 (meV)	—	59.4	88.0
GaN FK2 (meV)	—	—	176.0
(GaAs + GaN) FK1 (meV)	—	94.9	—
$\epsilon(\infty)$	10.9	10.3	5.4
$\epsilon(0)$	12.9	12.6	9.9
$\omega_{TO_{GaAs}}$ (meV)	32.8	32.8	—
$\omega_{TO_{GaN}}$ (meV)	—	58.8	66.1

of a nitrogen atom in a GaAs lattice. The peak at 59.4 meV in the $GaN_{0.104}As_{0.896}$ spectra has a high energy-loss shoulder that is due to the overtone of the GaAs-like FK phonon at 71.0 meV. The remaining feature of the spectra, a low intensity peak at 94.9 meV, is attributed to a combination mode of GaAs-like and GaN-like FK1 phonons. This peak is visible in figure 8(c), where the intensity scale has been magnified for loss energies greater than 80 meV.

The exchange of energy between the probing electrons and the polarization field arising from the collective excitations of the lattice results from long range Coulomb interaction and can be described by the semiclassical dielectric theory within the methodology of Lambin *et al* [22]. Firstly, the single-scattering classical loss probability spectrum of the target is computed for an electron travelling along a specularly reflected trajectory. In this spectrum ((a) in figure 8), only two single-loss peaks appear, the GaAs-like and GaN-like FK phonon

modes; no gain peaks or multiple excitations are present. The complete electron-energy-loss spectrum, which includes multiple-scattering events for a non-zero target temperature, is then obtained via a Bose–Einstein thermodynamic average of the quantized surface excitations. This is shown as spectrum (b) in figure 8, where the GaAs-like and GaN-like FK phonon peaks can again be seen. The multiple-excitation modes are now apparent, with the overtone of the GaAs-like FK phonon peak at 71.0 meV and the combination mode of GaAs-like plus GaN-like FK phonon at 94.9 meV being reproduced. Direct comparison of this computed spectrum with experimental data is then made possible by performing a convolution with a model of the instrumental response of the spectrometer. The resulting final simulation is shown as a solid curve in spectrum (c) in figure 8 with the experimental data. The dielectric function used to simulate the experimental HREEL spectra recorded from $GaN_{0.104}As_{0.896}$ is

$$\epsilon(\omega) = \epsilon(\infty) + x\left[\frac{[\epsilon(0) - \epsilon(\infty)]\,\omega_{\mathrm{TO_{GaN}}}^2}{\omega_{\mathrm{TO_{GaN}}}^2 - \omega^2 - \mathrm{i}\gamma_{\mathrm{GaN}}\omega}\right] + (1-x)\left[\frac{[\epsilon(0) - \epsilon(\infty)]\,\omega_{\mathrm{TO_{GaAs}}}^2}{\omega_{\mathrm{TO_{GaAs}}}^2 - \omega^2 - \mathrm{i}\gamma_{\mathrm{GaAs}}\omega}\right] \tag{4}$$

where the parameters are defined as for equation (2) and the dielectric function has three components, for the background, the GaAs-like and the GaN-like FK phonons. A composition-dependent prefactor has also been inserted before each phonon term. The static and high frequency dielectric constants used in this expression have been linearly interpolated for $GaN_{0.104}As_{0.896}$ using the GaAs and GaN values as end points. Since wurtzite GaN is anisotropic, effective dielectric constants $\epsilon_{\mathrm{eff}} = \sqrt{\epsilon_\perp \epsilon_\parallel}$ have been used, where $\epsilon_\perp$ and $\epsilon_\parallel$ denote the dielectric constants perpendicular and parallel to the c-axis, respectively [37]. The results of the HREELS simulations are shown in figures 7 and 8. The simulations of the GaAs and GaN spectra were performed using a dielectric function with a single-phonon term. As all of the samples were undoped, no plasmon term was required in the dielectric functions to simulate energy loss due to conduction band electron plasmon excitations. The dielectric constants and transverse optical phonon frequencies used in all of the simulations are given in table 2.

Using $x = 0.104$ in the dielectric function (equation (4)), the simulations accurately reproduce both the position and intensity of all the observed loss peaks. This x value is in agreement with nitrogen content determined from XRD analysis. Changing this value of x by more than 0.01 in the dielectric function resulted in simulations that deviated significantly from the experimental spectra. The shift to lower loss energy of the GaAs-like FK phonon peak in the $GaN_{0.104}As_{0.896}$ spectra is reproduced in the simulations using the same transverse optical phonon frequency for the mode as for GaAs, by virtue of the nitrogen-induced changes to the dielectric constants. A slightly lower transverse optical phonon frequency was used for the GaN-like mode in $GaN_{0.104}As_{0.896}$ than for pure GaN. This is because the local GaN vibrational frequency is influenced by the surrounding lattice. The localized mode frequency of a nitrogen atom in a GaAs lattice is lower than the mode frequency of nitrogen in GaN.

6. Conclusions

The potential of electron spectroscopies for the investigation of a wide range of properties of dilute nitrides has been demonstrated. Core level photoelectron spectroscopy has been used to study the nitrogen bonding configurations in dilute III–N–V alloys. Post-growth XPS analysis can determine why nitrogen contents obtained by XRD analysis and SIMS disagree. While only N–In bonding was found in InN_xAs_{1-x} alloys, several nitrogen bonding configurations were observed in InN_xSb_{1-x} alloys.

Nitrogen in the dilute InN_xSb_{1-x} alloys grown using a mixed nitrogen and hydrogen plasma has been found to be bonded to both In and Sb, and is also located in N–H complexes. This explains the origins of the disagreement between compositions determined by SIMS and XRD analysis. Annealing for 8 h at 300 °C partially removes hydrogen from N–H complexes and increases the amount of N bonded to In. Plasma frequency measurements using HREELS indicate that annealing decreases the conduction electron concentration. This is due to the annealing removing H from neutral N–H complexes, leaving a greater concentration of isoelectronic N acceptors, and may also be due to the annealing repairing donor-like defects.

The surface optical FK phonon spectra of GaN_xAs_{1-x} have been investigated by HREELS. Multiple excitations of both GaAs-like and GaN-like modes were observed. The localized mode frequency of the GaN-like FK phonons in GaN_xAs_{1-x} of 59.0 meV is very close to the LO_2 bulk phonon band or local vibrational mode previously observed in this alloy by means of Raman scattering. The experimental spectra have been accurately simulated using semiclassical dielectric theory. The phonon terms used in the dielectric function contain composition-dependent coefficients whose values are in agreement with the composition determined from XRD analysis.

Acknowledgments

The authors would like to thank Dr Hai Lu and Dr Bill Schaff of Cornell University, Ithaca, NY, USA, for the provision of the InN samples. We are also grateful to Dr Danny Law and Dr Graham Beamson of the National Centre for Electron Spectroscopy and Surface (NCESS) analysis for their assistance with the XPS experiments. Finally, we acknowledge the Engineering and Physical Sciences Research Council, UK, for studentships under the doctoral training account scheme, for financial support under grants GR/R93872/01 and GR/S56030/01 and for access to the NCESS facility under grant GR/S14252/01.

References

[1] Buyanova I A, Chen W M and Monemar B 2001 *MRS Internet J. Nitride Semicond. Res.* **2** 2
[2] Kondow M, Uomi K, Niwa A, Kitatani T, Watahiki S and Yazawa Y 1996 *Japan. J. Appl. Phys.* 2 **35** 1273
[3] Margaritondo G 1993 *J. Vac. Sci. Technol.* B **11** 1362
[4] Margaritondo G 1999 *Rep. Prog. Phys.* **62** 765
[5] Kitatani T, Kondow M, Kikawa T, Yazawa Y, Okai M and Uomi K 1999 *Japan. J. Appl. Phys.* 1 **38** 5003
[6] Ashley T, Burke T M, Pryce G J, Adams A R, Andreev A, Murdin B N, O'Reilly E P and Pidgeon C R 2003 *Solid-State Electron.* **47** 387
[7] Johnson A D, Bennett R H, Newey J, Pryce G J, Williams G M and Burke T M 2000 *Mater. Res. Soc. Symp. Proc.* **607** 23
[8] Murdin B N, Kamal-Saadi M, Lindsay A, O'Reilly E P, Adams A R, Nott G J, Crowder J G, Pidgeon C R, Bradley I V, Wells J-P R, Burke T, Johnson A D and Ashley T 2001 *Appl. Phys. Lett.* **78** 1568
[9] Shih D-K, Lin H-H, Sung L-W, Chu T-Y and Yang T-R 2003 *Japan. J. Appl. Phys.* 1 **42** 375
[10] Hung W K, Cho K S, Chern M Y, Chen Y F, Shih D K, Lin H H, Lu C C and Yang T R 2002 *Appl. Phys. Lett.* **80** 796
[11] Wang J-S and Lin H-H 1999 *J. Vac. Sci. Technol.* B **17** 1997
[12] Wang J-S, Lin H-H, Song L-W and Chen G-R 2001 *J. Vac. Technol.* B **19** 202
[13] Veal T D, Mahboob I and McConville C F 2003 *Appl. Phys. Lett.* **83** 1776
[14] Li W, Pessa M and Likonen J 2001 *Appl. Phys. Lett.* **78** 2864
[15] Fan W J, Yoon S F, Ng T K, Wang S Z, Loke W K, Liu R and Wee A 2002 *Appl. Phys. Lett.* **80** 4136
[16] Spruytte S G, Coldren C W, Harris J S, Wampler W, Krispin P, Ploog K and Larson M C 2001 *J. Appl. Phys.* **89** 4401
[17] Hecht J-D, Frost F, Hirsch D, Neumann H, Schindler A, Preobrajenski A B and Chassé T 2001 *J. Appl. Phys.* **90** 6066

[18] Zhang J-P, Sun D-Z, Wang X-L, Kong M-Y, Zeng Y-P, Li J-M and Lin L-Y 1999 *Semicond. Sci. Technol.* **14** 403
[19] Liu H, Bertolet D C and Rogers J W Jr 1994 *Surf. Sci.* **320** 145
[20] Mahboob I, Veal T D and McConville C F 2003 *Appl. Phys. Lett.* **83** 2169
[21] Veal T D and McConville C F 2001 *Phys. Rev.* B **64** 085311
[22] Lambin Ph, Vigneron J P and Lucas A A 1985 *Phys. Rev.* B **32** 8203
[23] O'Reilly E P and Lindsay A 1999 *Phys. Status Solidi* b **216** 131
[24] Lindsay A and O'Reilly E P 2001 *Solid State Commun.* **118** 313
[25] Lindsay A 2003 private communication
[26] Xin H P, Tu C W and Geva M 2000 *J. Vac. Sci. Technol.* **18** 1476
[27] Hopfield J J, Thomas D G and Lynch R T 1966 *Phys. Rev. Lett.* **17** 312
[28] Janotti A, Zhang S B, Wei S H and Van de Walle C G 2002 *Phys. Rev. Lett.* **89** 086403
[29] Fuchs R and Kliewer K L 1965 *Phys. Rev.* A **140** 2076
[30] Ibach H 1970 *Phys. Rev. Lett.* **24** 1416
[31] Lambin Ph, Vigneron J P, Lucas A A, Thiry P A, Liehr M, Pireaux J J, Caudano R and Kuech T J 1986 *Phys. Rev. Lett.* **56** 1842
[32] Thiry P A, Liehr M, Pireaux J J, Caudano R and Kuech T J 1986 *J. Vac. Sci. Technol.* A **4** 953
[33] Prokofyeva T, Sauncy T, Seon M, Holtz M, Qiu Y, Nikishin S and Temkin H 1998 *Appl. Phys. Lett.* **73** 1409
[34] Matz R and Lüth H 1981 *Phys. Rev. Lett.* **46** 500
[35] Mintairov A M, Blagnov P A, Melehin V G, Faleev N N, Merz J L, Qiu Y, Nikishin S A and Temkin H 1997 *Phys. Rev.* B **56** 15836
[36] Klar P J, Grüning H, Chen L, Hartmann T, Golde D, Güngerich M, Heimbrodt W, Koch J, Volz K, Kunert B, Torunski T, Stolz W, Polimeni A, Capizzi M, Dumitras Gh, Gelhaar L and Riechert H 2003 *IEE Proc. Optoelectron.* **150** 28
[37] Grabowski S P, Kampden T U, Nienhaus H and Mönch W 1998 *Appl. Surf. Sci.* **123/124** 33